Advances in Nano Research, *Vol. 10, No. 5 (2021) 415-422*
DOI: https://doi.org/10.12989/anr.2021.10.5.415

Low-dimensional modelling of n-type doped silicene and its carrier transport properties for nanoelectronic applications

M.W. Chuan, J.Y. Lau, K.L. Wong, A. Hamzah, N.E. Alias, C.S. Lim and M.L.P Tan*

School of Electrical Engineering, Faculty of Engineering, Universiti Teknologi Malaysia, 81310 Skudai, Johor, Malaysia

(*Received September 4, 2020, Revised January 4, 2021, Accepted January 5, 2021*)

Abstract. Silicene, a 2D allotrope of silicon, is predicted to be a potential material for future transistor that might be compatible with present silicon fabrication technology. Similar to graphene, silicene exhibits the honeycomb lattice structure. Consequently, silicene is a semimetallic material, preventing its application as a field-effect transistor. Therefore, this work proposes the uniform doping bandgap engineering technique to obtain the n-type silicene nanosheet. By applying nearest neighbour tight-binding approach and parabolic band assumption, the analytical modelling equations for band structure, density of states, electrons and holes concentrations, intrinsic electrons velocity, and ideal ballistic current transport characteristics are computed. All simulations are done by using MATLAB. The results show that a bandgap of $0.66\,eV$ has been induced in uniformly doped silicene with phosphorus (PSi_3NW) in the zigzag direction. Moreover, the relationships between intrinsic velocity to different temperatures and carrier concentration are further studied in this paper. The results show that the ballistic carrier velocity of PSi_3NW is independent on temperature within the degenerate regime. In addition, an ideal room temperature subthreshold swing of $60\,mV/dec$ is extracted from ballistic current-voltage transfer characteristics. In conclusion, the PSi_3NW is a potential nanomaterial for future electronics applications, particularly in the digital switching applications.

Keywords: doped silicon; bandgap engineering; 2D material; nanoelectronics; ballistic current transport

1. Introduction

International Roadmap of Devices and Systems (IRDS) is a 15 years roadmap on the development and growth of electronic devices and systems in the micron and nanometer regime. The 'more than Moore Chapter' in IRDS, predicts that there is no more headroom for 2D geometry scaling and 3D very large-scale integration (VLSI) of circuits and systems using stacked integration approach after the year 2027 (IEEE 2018). Thus, this major challenge has urged the semiconductor industry to discover potential "more than Moore' materials, in order to achieve higher computing power. Due to the success on the exploration of graphene (Novoselov *et al*. 2004), researchers are interested in studying and exploring other 2D materials, including silicene. Silicene is known as a potential 2D material besides graphene. It is a monolayer allotrope of silicon (Si) arranged in honeycomb lattice structure like graphene (Ding and Ni 2009). Moreover, the atomically thin 2D materials are postulated to enable a new generation of nanoelectronic devices, such as wearable and flexible electronics (Gupta *et al*. 2015, Chhowalla *et al*. 2016)

Silicene has similar Dirac cone properties and lattice structure like graphene, and these unique properties result in an ultra-high carrier mobility. Moreover, silicene has zero bandgap when the spin orbiting effect is neglected (Lew Yan Voon *et al*. 2016). This unique characteristic can be observed in the electronic dispersion relation as shown in the published results from other researchers (Guzmán-Verri and Lew Yan Voon 2007, Ding and Wang 2013, Huang *et al*. 2013). Meanwhile, the mean free path (MFP) of monolayer silicene for acoustic and optical phonon scattering are $178\,nm$ and $29\,nm$ (Wang *et al*. 2015), respectively. The next generation devices might be able to operate under ballistic or near-ballistic transport due to these short MFP values (Arora *et al*. 2007). Furthermore, the valence band and conduction band of the pristine silicene touch each other at the K-point within the first Brillouin zone (Guzmán-Verri and Lew Yan Voon 2007, Ding and Wang 2013, Huang *et al*. 2013, Gert *et al*. 2015). This semimetallic property of silicene hinders its potential as a field-effect transistors (FETs) where the channel materials require band gap values between $0.4\,eV$ (Ni *et al*. 2014) and $3\,eV$ (Tang and Zhou 2013). Although graphene is an established 2D material with mature knowledge in the research community, silicene offers potential advantages in terms of the fabrication processes because Si-based technology is well known and dominant in the semiconductor industry (Tao *et al*. 2015).

Meanwhile, experimentalists are constantly working to explore practical fabrication procedures to produce silicene in the laboratory. Unlike graphene which can be mechanically exfoliated from its bulk graphite, molecular beam epitaxial (MBE) growth is identified as the most viable technique to fabricate silicene (Molle *et al*. 2018). In the past decade, most of the experimental work have been focusing on depositing silicene on metal substrates such as silver (Vogt *et al*. 2012)

*Corresponding author, Ph.D.,
E-mail: michael@utm.my

ISSN: 2287-237X (Print), 2287-2388 (Online)

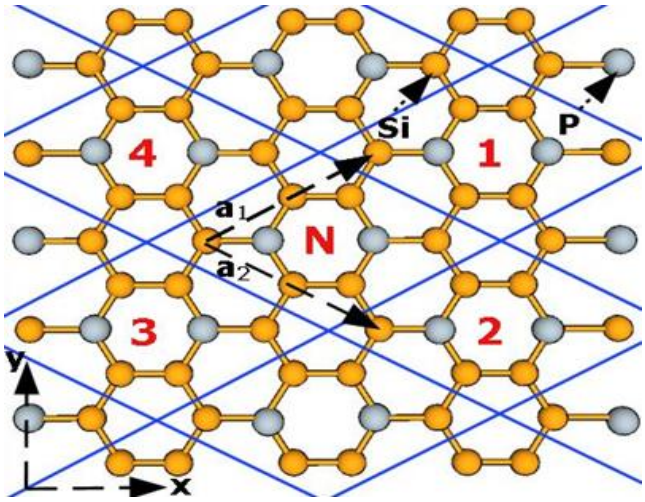

Fig. 1 Schematic lattice structure of 2D PSi_3, a_1 and a_2 denotes the displacement vectors, each parallelogram shows a primitive unit cell of PSi_3.

and gold (Stpniak-Dybala *et al*. 2019). At any rate, the search for suitable non-metallic substrate is more favourable by the research community due to wider practical applications (Le Lay *et al*. 2018).

Recently, various bandgap opening techniques are studied in order to tune the semimetallic properties of silicene (Chuan *et al*. 2020b). For example, band gap opening techniques for 2D materials like substitutional doping (Lopez-Bezanilla 2014, Ma *et al*. 2014), incorporating defects (Gao, Zhang *et al*. 2013, Ali, Pi *et al*. 2017, Wong *et al*. 2019), strain engineering (Mohan *et al*. 2014, Voon *et al*. 2015) and others have been studied. Among all these techniques, substitutional doping is a typical way used in the semiconductor fabrication industry to design a device based on the desired applications (Taur *et al*. 1995).

This work is primarily motivated by the published DFT results (Ding and Wang 2013) where sizable band gap values are discovered in silicene by applying substitutional doping with n-type material, phosphorus (P) at a constant concentration, referred as PSi_3 nanostructure in the article. However, there is still lack of details on other important electronics properties and carrier transport properties for PSi_3 nanostructure. In addition, theoretical and computational studies are relatively important (Bouadi *et al*. 2018) because there are still major challenges in the fabrications of free-standing silicene (Balendhran *et al*. 2015).

In this paper, an analytical model based on the tight-binding and parabolic band assumption is employed to investigate the essential electronic and carrier transport parameters of 1D PSi_3 nanoribbon (PSi_3NW) as shown in Fig. 1. In Section 2, the mathematical modelling of band structure, density of states (DOS), carrier concentration, intrinsic velocity and ballistic current-voltage (I-V) characteristics of PSi_3NW using nearest neighbour tight-binding (NNTB) approach and parabolic band assumption are shown. In Section 3, all the simulation results obtained are shown and analysed. Lastly in Section 4, the conclusion is drawn based on the findings of this work.

2. Mathematical modelling

2.1 Band structure and density of states of PSi_3NW

Fig. 1 shows the sketched lattice diagram of the 2D PSi_3 with the corresponding displacement vectors to its nearest neighbours, defined as $\overrightarrow{a_1}$ and $\overrightarrow{a_2}$. The PSi_3 nanosheet is assumed to be a perfect planar lattice structure. This assumption is employed because planar silicene has been successfully fabricated recently (Stpniak-Dybala *et al*. 2019), despite the mainstream buckled structure. Every primitive unit cell interacts with its four nearest neighbour unit cells. The remaining displacement vectors in the opposite direction are the complex conjugate of $\overrightarrow{a_1}$ and $\overrightarrow{a_2}$. For NNTB, the time-independent Schrödinger equation was applied in the matrix form (Datta 2005), given as

$$E(\emptyset_0) = [h(\vec{k})](\emptyset_0) \tag{1}$$

where E is the energy, $\emptyset_0$ and $[h(\vec{k})]$ show the wave function and the Hamiltonian operator in matrix form, respectively. The Hamiltonian operator matrix is obtained from the summation all non-zero overlap components for m in positive integers among all the nearest neighbour unit cells by using:

$$[h(\vec{k})] = \sum_{m=n,1}^{4} H_{nm} e^{i\vec{k}\cdot(\vec{r}_n - \vec{r}_m)} \tag{2}$$

where $\vec{k}$ as the wave vector, H_{nm} is the Hamiltonian matrix for every neighbouring unit cell, $\vec{r}_n$ and $\vec{r}_m$ are the position vectors used to determine the displacement of m^{th} unit cell from n^{th} unit cell. The origin could be placed at any atom of n^{th} unit cell. In this work, the n^{th} unit cell is defined as the unit cell labelled letter 'N' in Fig 1. After obtaining the Hamiltonian matrices for unit cell: H_{nn} and the nearest neighbours: H_{n1}, H_{n2}, H_{n3}, and H_{n4}, apply Eq. (2) to obtain the complete Hamiltonian matrix as

$$[h(\vec{k})] = \begin{bmatrix} E_{oSi} & 0 & 0 & \boldsymbol{t_{P-Si}} & 0 & h_1^* & h_2^* & 0 \\ 0 & E_{oSi} & 0 & \boldsymbol{t_{P-Si}} & 0 & 0 & t_{Si-Si} & h_1^* \\ 0 & 0 & E_{oSi} & \boldsymbol{t_{P-Si}} & 0 & t_{Si-Si} & 0 & h_2^* \\ \boldsymbol{t_{P-Si}} & \boldsymbol{t_{P-Si}} & \boldsymbol{t_{P-Si}} & \boldsymbol{E_{oP}} & 0 & 0 & 0 & 0 \\ 0 & 0 & 0 & 0 & \boldsymbol{E_{oP}} & \boldsymbol{t_{P-Si}} & \boldsymbol{t_{P-Si}} & \boldsymbol{t_{P-Si}} \\ h_1 & 0 & t_{Si-Si} & 0 & \boldsymbol{t_{P-Si}} & E_{oSi} & 0 & 0 \\ h_2 & t_{Si-Si} & 0 & 0 & \boldsymbol{t_{P-Si}} & 0 & E_{oSi} & 0 \\ 0 & h_1 & h_2 & 0 & \boldsymbol{t_{P-Si}} & 0 & 0 & E_{oSi} \end{bmatrix} \tag{3}$$

where $h_1 = t_{Si-Si} e^{i(ak_x - bk_y)}$ and $h_2 = t_{Si-Si} e^{i(ak_x + bk_y)}$. E_{oSi} and E_{oP} represent the on-site or bounded energy for Si and P atom, respectively, t_{P-Si} is the hopping energy for P-Si atoms, and t_{Si-Si} is the hopping energy for Si-Si atoms. h_1^* and h_2^* is the complex conjugate of h_1 and h_2, respectively. The bold terms in Eq. (3) show the influence of doping atoms (P) to the Hamiltonian matrix of silicene.

Table 1 tabulates the NNTB parameters used in this work: t_{P-Si} by fitting DFT result, t_{Si-Si} from (Chuan *et al*. 2020a, Chuan *et al*. 2020c), and both the E_{oSi} and E_{oP} from (Harrison 2004). After that, the band structure is assumed be confined in the x-direction as explained by (Lim, Hamzah *et al*. 2017b) to obtain 1D PSi_3NW in the zigzag direction. Then, Eq. (3) is substituted into Eq. (1) to obtain the energy eigenvalue equation. By solving the

Table 1 The compute NNTB model parameters for uniformly doped silicene

Parameters	t_{Si-Si}	t_{P-Si}	E_{oSi}	E_{oP}
Value (eV)	-1.02	-1.16	-7.59	-9.54

energy eigenvalue equation using the equation: $\det\left|[h(\vec{k})] - EI\right| = 0$, the energy eigenvalues are obtained.

Next, to obtain a simple analytical model for carrier characteristics of PSi_3NW (Lundstrom and Antoniadis 2014), parabolic band assumption is applied around the conduction band minimum (CBM) and valence band maximum (VBM) (Ismail *et al*. 2016) as these bands are the responsible for carrier flow in semiconductor. The parabolic band assumption originates from the effective mass equations such that the wave functions in the Schrödinger equation do not appear explicitly (Datta 1997) to simplify the modelling procedures, the parabolic band equations are

$$E_e(k) = E_c + \frac{\hbar^2 k^2}{2m_e{}^*} \tag{4a}$$

$$E_h(k) = E_v - \frac{\hbar^2 k^2}{2m_h{}^*} \tag{4b}$$

where E_c and E_v represent the energies at CBM and VBM, respectively, $m_e{}^*$ and $m_h{}^*$ are the effective mass for electrons and holes, respectively, and $\hbar = h/(2\pi)$ is the reduced Planck's constant.

Density of states (DOS), describing the number of available states with respect to energy E, can be derived applying Eq. (5) to the parabolic band structure Eqs. (4a) and (4b) (Lim *et al*. 2017a), expressed as

$$DOS(E) = \frac{\Delta N_x}{L_x \Delta E} \tag{5}$$

where N_x is the total number of states, L_x is the length and E is the energy. The resulting DOS for carriers are obtained as

$$DOS_e(E) = \sqrt{\frac{2m_e{}^*}{\pi^2\hbar^2}}(E - E_c)^{-1/2} \tag{6a}$$

$$DOS_h(E) = \sqrt{\frac{2m_h{}^*}{\pi^2\hbar^2}}(E_v - E)^{-1/2} \tag{6b}$$

where the DOS for electron (DOS_e) and DOS for hole (DOS_h) are derived using Eqs. (4a) and (4b), respectively.

2.2 Carrier concentration of PSi_3NW

In this subsection, the concentrations for electrons and holes in CBM and VBM are derived. The probability of the occupied states at a given temperature, T can be described by Fermi-Dirac distribution (Lundstrom and Jeong 2013)

$$f(E) = \left[1 + \exp\left(\frac{E - E_F}{k_B T}\right)\right]^{-1} \tag{7}$$

where k_B represents the Boltzmann constant. Thermal equilibrium or intrinsic electrons concentration (Jooq *et al*. 2018) available in the conduction band is calculated using

$$n = \int_0^\infty DOS_e(E) f(E)\, dE = N_c \Im_{-1/2}(\eta_c) \tag{8}$$

where $\Im_{-1/2}(\eta_c)$ is the Fermi-Dirac integral (FDI) of order $-1/2$ with respect to η_c, N_c represents the effective DOS of electrons in terms of normalised thermal energy, $\eta_c = (E_F - E_c)/k_B T$, and is given by $N_c = \sqrt{(2m_e{}^* k_B T)/\pi\hbar^2}$. The general equation for FDI of order j (Kim and Lundstrom 2008) is given by

$$\Im_j(\eta) \equiv \frac{1}{\Gamma(\mathrm{j}+1)} \int_0^\infty \frac{\varepsilon^j\, d\varepsilon}{1 + e^{\varepsilon - \eta}} \tag{9}$$

where Γ denotes the gamma function. Eq. (9) is crucial and used throughout the rest of this paper. In a similar way, the intrinsic (which is also known as thermal equilibrium) holes concentration in the valence band can be calculated using

$$p = \int_{-\infty}^0 DOS_h(E)[1 - f(E)]\, dE = N_v \Im_{-1/2}(\eta_v) \tag{10}$$

where the effective density of states of holes, N_v, and normalised energy in terms of thermal energy η_v are given by $N_v = \sqrt{(2m_h{}^* k_B T)/\pi\hbar^2}$ and $\eta_v = (E_v - E_F)/k_B T$, respectively. Note that for holes concentration in the valence band, $f(E)$ is substituted by $[1 - f(E)]$ to compute the probability of empty states.

FDI usually can be separated and divided into two regimes which are non-degenerate and degenerate regimes that reduces Eq. (9) into $\Im_j(\eta) = e^\eta$ for $(\eta < -2)$ regardless of j and $\Im_j(\eta) = \eta^{j+1}/[(\mathrm{j}+1)\Gamma(\mathrm{j}+1)]$ for $(\eta \geq 3)$ respectively (Johari, Ahmadi *et al*. 2010). The numerical solutions for FDI in this work are based on the available Matlab function on nanohub.org (Kim and Lundstrom 2008).

2.3 Intrinsic carrier velocity of PSi_3NW

From this subsection onwards, the focus is on the electrons as the carriers in the PSi_3NW nanostructure. The intrinsic velocity of electrons is obtained by dividing the total electrons velocity by the electrons concentration (Arora 2015), given as

$$\frac{\int_0^\infty |v_e(E)| DOS_e(E) f(E)\, dE}{\int_0^\infty DOS_e(E) f(E)\ dE} \tag{11}$$

where $|v_e(E)| = \sqrt{2(E - E_v)/m_e{}^*}$ is the average magnitude of electron velocity. Using Eqs. (8) and (9), (11) can be simplified to become

$$v_{ie} = v_{thn} \frac{\Im_0(\eta_c)}{\Im_{-1/2}(\eta_c)} \tag{12}$$

where $v_{thn} = \sqrt{2k_B T/\pi m_e{}^*}$ is the thermal velocity of electrons for PSi_3NW.

2.4 Current-voltage characteristics of PSi_3NW

With the electronic and carrier transport properties, the model is now ready to be simulated using the Landauer-Büttiker ballistic current equation, by introducing an ideal gate potential $U \equiv -q|V_{bias}|$ within the PSi_3NW channel. Due to the n-type nature of PSi_3NW, the current transport equation will be based on the n-channel metal-oxide-semiconductor field-effect transistor (MOSFET) where electrons are the majority charge carrier in the semiconducting channel, noting that the working principles of the 2D MOSFETs are similar to those of the junctionless FETs (Schwierz *et al*. 2015). By assuming ideal metal contacts and high drain bias (Supriyo 2017, Chuan *et al*. 2020c), the I-V characteristic for PSi_3NW can be expressed as

$$I_{DS} = \frac{q}{2}\int_0^{\infty} |v_e(E)|DOS_e(E)f_s(E+U)\,dE = \frac{qN_c v_{thn}}{2}\Im_0\left[\frac{E_F + q|V_{bias}| - E_c}{k_B T}\right] \quad (13)$$

by using Eqs. (8) and (12), where V_{bias} is introduced as the ideal biasing voltage to control the channel potential U, and f_s is the Fermi energy level at the source terminal.

3. Result and discussion

3.1 Band structure and density of states of PSi_3NW

Fig. 2 shows the normalised band structure of PSi_3NW. From the band structure, a bandgap value is extracted, by computing the difference between CBM and VBM

$$E_g = |CBM - VBM| \quad (14)$$

The CBM and VBM extracted from the band structure of PSi_3NW are $0.33\,eV$ and $-0.33\,eV$ respectively. As a result, the bandgap for PSi_3NW is $0.66\,eV$.

This bandgap value is slightly higher from the previous research ($E_g = 0.58\,eV$) by Ding *et al*. (2013) because the PSi_3NW in this work is assumed as a perfect planar lattice structure based on one-dimensional basis. Despite this slight deviation, the extracted bandgap energy is still suitable for the applications in the areas of nanoelectronics based on the standard value of bandgap, which between $0.4\,eV$ (Ni *et al*. 2014) and $3\,eV$ (Tang and Zhou 2013). The benchmark for band gap values are tabulated in Table 2.

Parabolic band assumption is applied around the CBM and VBM to obtain the effective mass for electrons and holes by fitting NNTB band structure. The obtained effective masses for electrons and holes are $m_e^* = 0.230m_0$ and $m_h^* = 0.240m_0$, respectively where m_0 is the electron rest mass constant. Fig. 3(a) illustrates that the parabolic band structure around the CBM and VBM of PSi_3NW is nicely fitted to the NNTB band structure. Fig. 3(b) shows the DOS plotted using Eqs. (6a) and (6b). From

Table 2 Benchmark of semiconductor bandgap values for nanoelectronics applications.

Materials	Min.	PSi_3	Bulk Si	Max.
Bandgap (eV)	0.40	0.66	1.12	3.00

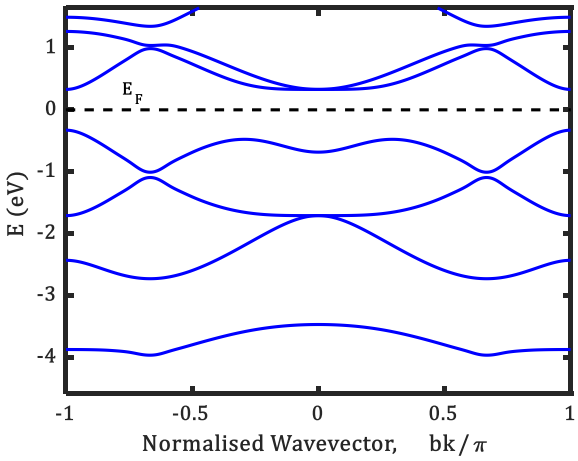

Fig. 2 Band diagram of PSi_3NW in the zigzag direction using NNTB model.

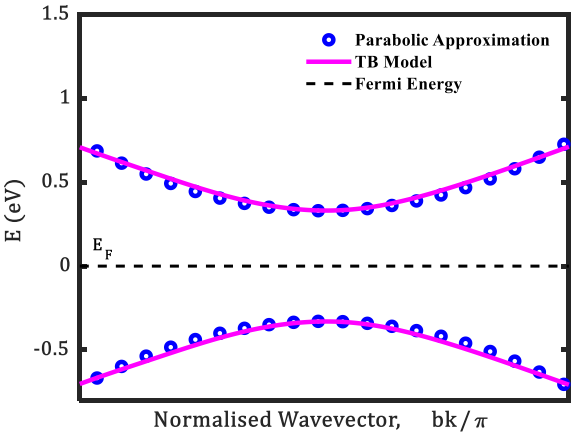

(a) Band structure

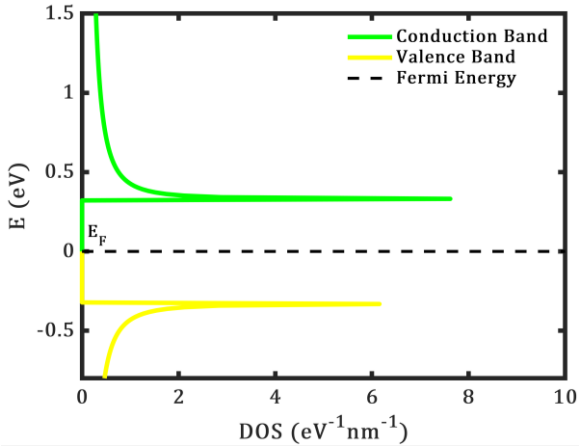

(b) DOS

Fig. 3 Band diagram and DOS of PSi_3NW using parabolic band assumption.

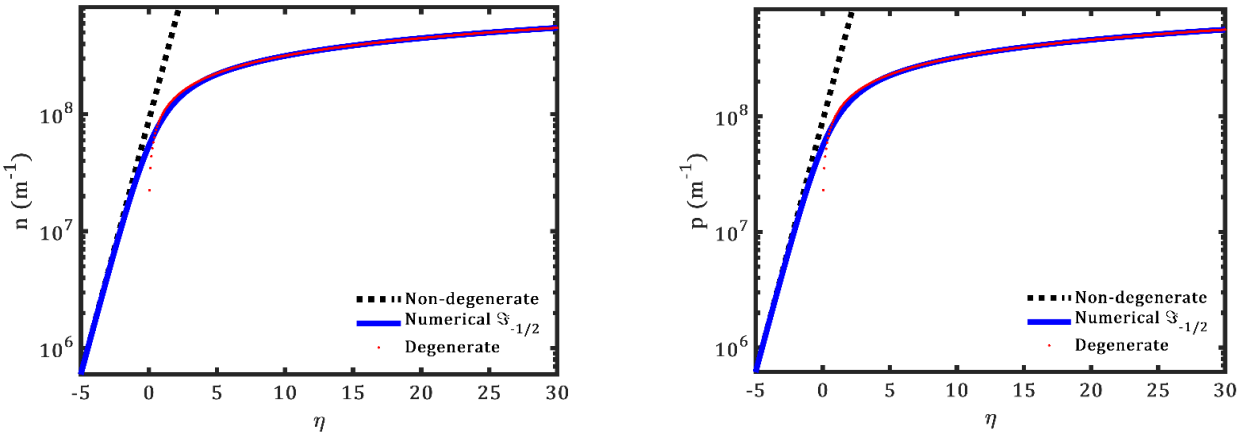

(a) Electron concentration (b) Hole concentration

Fig. 4 Carrier concentrations of PSi_3NW with respect to the normalized Fermi energy, η within the both regimes.

the DOS, it is shown that the peaks of DOS occur at the minimum point of conduction band and the maximum point of the valence band. The Fermi energy level E_F is set to zero in this work.

3.2 Carrier concentration of PSi_3NW

Figs. 4(a) and 4(b) show the intrinsic carrier concentrations of electrons and holes respectively for both the exact numerical FDI and reduced FDI calculations. From the graph, degenerate carrier concentration for electrons at $\eta_c = 3$ is extracted where $n = 1.739 \times 10^8\ m^{-1}$ and for holes $\eta_v = 3$ is $p = 1.786 \times 10^8\ m^{-1}$. At the degenerate regime, the electrons and holes concentrations start to saturate and do not have significant variations.

3.3 Intrinsic carrier velocity of PSi_3NW

The intrinsic or thermal equilibrium velocities for electrons are computed and plotted. Fig. 5 shows the graph of intrinsic velocity for electrons versus temperature for three different electrons concentrations: $n = 1 \times 10^4\ m^{-1}$ for non-degenerate regime, $n = 2 \times 10^8\ m^{-1}$ and $n = 5 \times 10^8\ m^{-1}$ for degenerate regime. From the results, the relationship of intrinsic electrons velocity versus temperature is obtained: the intrinsic electrons velocity, v_{ie} is proportional to the temperature by $T^{0.5}$.

As depicted in Fig. 6, the intrinsic velocity for electrons remains almost constant at non-degenerate regime where $n < 1 \times 10^8\ m^{-1}$. Interestingly, it is observed that the intrinsic electron velocity v_{ie} is increasing without dependence on the temperature at the degenerate regime where $n > 1 \times 10^8\ m^{-1}$ (which is clearly shown is the dashed oval in Fig. 6). The intrinsic electrons velocity v_{ie} has become a simple function which merely depends on the electrons concentrations. This unique relationship (the independence of temperature at the degenerate regime) is consistent with the results in previous study involving 1D nanostructures (Ahmadi *et al.* 2009, Lim *et al.* 2018). Nevertheless, these findings are limited to devices within the ballistic transport regimes where the lengths of the devices are smaller than the MFP of the material.

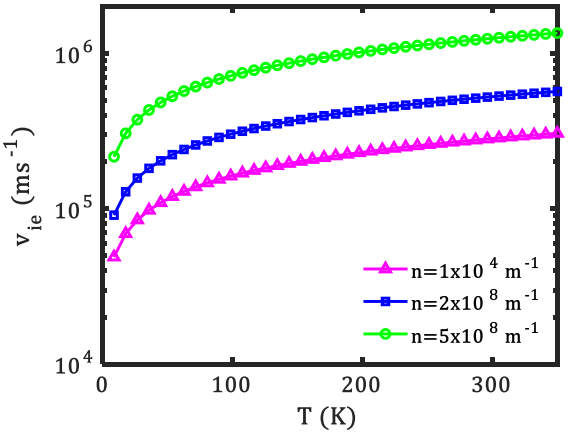

Fig. 5 Electrons intrinsic velocity versus the temperature of PSi_3NW for three different electrons concentrations.

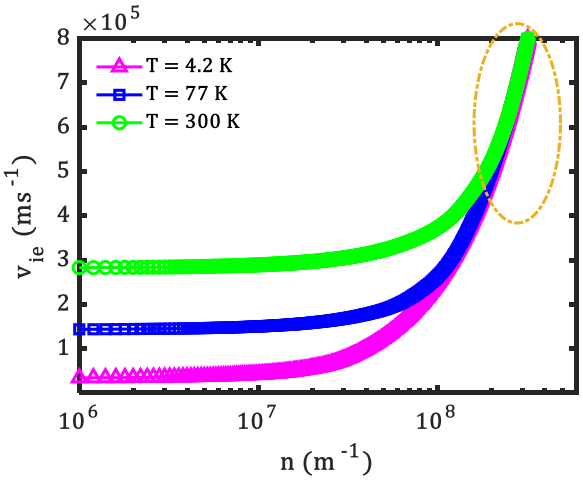

Fig 6. Electrons intrinsic velocity versus the carrier concentration of PSi_3NW at various temperature, including ambient temperature, T = 300 K.

3.4 Current-voltage characteristics of PSi_3NW

Fig. 7(b) compares the transfer characteristics of p-typedoped silicene using aluminium dopant atoms from

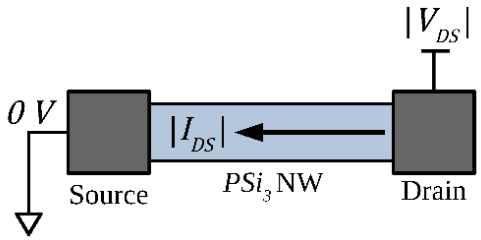

(a) PSi_3NW ballistic current model

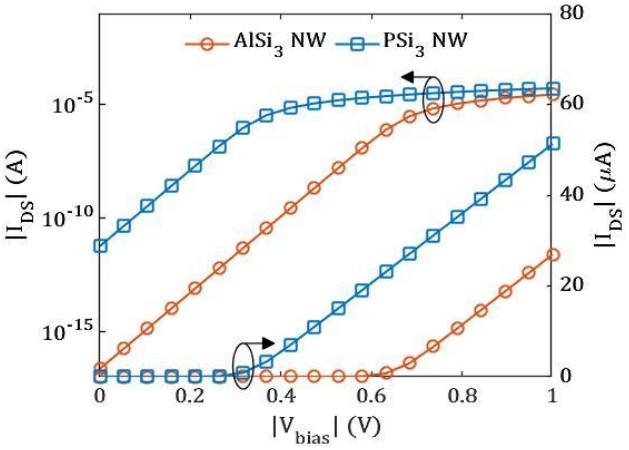

(b) Transfer characteristics

Fig. 7 (a) Schematic diagram of I-V characteristic model; and (b) Comparison of I–V characteristics between PSi_3NW of the proposed model and $AlSi_3NW$ adapted from (Chuan, Wong *et al*. 2020c).

(Chuan *et al*. 2020c) and n-type doped silicene using phosphorus dopant atoms in this work. Under this ideal ballistic transport condition, both models have achieved the ideal subthreshold swing, $SS = \Delta V_{bias}/\Delta log_{10} I$ of $60\, mV/dec$ at room temperature, $T = 300\, K$. However, the threshold voltage, V_{th1} obtained for PSi_3NW is about 50% of the V_{th2} obtained for $AlSi_3NW$, where $V_{th1} = 0.32\, V$ and $V_{th2} = 0.65\, V$. In a practical MOSFET device, these threshold voltages can be adjusted by tuning the work function of the gate metal and the source doping density. The results in Fig. 7(b) clearly show that the uniformly doped silicene could function as the channel materials for FET application. In future work, these nanostructures could be applied as the channels of FETs using transistor models such as the top-of-the-barrier nanotransistor model (Rahman *et al*. 2003, Chuan *et al*. 2020d, Chuan *et al*. 2021). Subsequently, the doped silicene could also be used for complementary metal-oxide-semiconductor (CMOS) technology, similar to previous studies on graphene (Banerjee *et al*. 2010, Goossens *et al*. 2017). The analytical equations computed in this work are useful for further device- and circuit-level modelling and simulations by creating SPICE models (Kazmierski *et al*. 2007).

4. Conclusion

In short, the proposed analytical model has achieved the objectives of this work where the electronic and carrier transport properties of PSi_3NW are computed. These properties include the band structure, density of states (DOS), intrinsic carrier concentration, intrinsic carrier velocity and ballistic I-V characteristics. A bandgap value of $0.66\, eV$ is successfully opened originally semimetallic pristine silicene by using uniform substitutional doping with phosphorus. The extracted results include the degenerate electrons and holes concentrations of PSi_3NW of $n = 1.739 \times 10^8\, m^{-1}$ and $p = 1.786 \times 10^8\, m^{-1}$, respectively. In addition, it is observed the electrons intrinsic velocity is proportional to $T^{0.5}$ at non-degenerate regime and eventually becomes independent of temperature at degenerate regime. This work suggests that uniformly n-type doping is a viable technique to open semiconducting bandgap in silicene. As a result, the material can be applied for future nanoelectronics applications, especially in the digital switching devices. In summary, these findings provide insights for future research such as modelling and simulations of PSi_3NW at the FET device and CMOS circuit level.

Acknowledgements

The authors acknowledge the Research Management Centre (RMC) of Universiti Teknologi Malaysia (UTM) for providing excellent support and a stimulating research environment. Mu Wen would like to convey his gratitude for the award of PhD Zamalah Scholarship from the School of Graduate Studies, UTM. Michael Tan would like to acknowledge the financial support from UTM Fundamental Research (UTMFR) (Vote no.: Q.J130000.2551.21H51), which allowed the smooth progress of this research.

References

Ahmadi, M.T., Lau, H.H., Ismail, R. and Arora, V.K. (2009), "Current–voltage characteristics of a silicon nanowire transistor", *Microelectron. J.*, **40**(3), 547-549. https://doi.org/10.1016/j.mejo.2008.06.060.

Ali, M., Pi, X., Liu, Y. and Yang, D. (2017), "Electronic and magnetic properties of graphene, silicene and germanene with varying vacancy concentration", *AIP Adv.*, **7**(4), 045308. https://doi.org/10.1063/1.4980836.

Arora, V.K. (2015), *Nanoelectronics: Quantum Engineering of Low-dimensional Nanoensembles*, CRC Press, Florida, U.S.A. https://doi.org/10.1201/9781315222516.

Arora, V.K., Tan, M.L., Saad, I. and Ismail, R. (2007), "Ballistic quantum transport in a nanoscale metal-oxide-semiconductor field effect transistor", *Appl. Phys. Lett.*, **91**(10), 103510. https://doi.org/10.1063/1.2780058.

Balendhran, S., Walia, S., Nili, H., Sriram, S. and Bhaskaran, M. (2015), "Elemental analogues of graphene: silicene, germanene, stanene, and phosphorene", *Small.*, **11**(6), 640-652. https://doi.org/10.1002/smll.201402041.

Banerjee, S.K., Register, L.F., Tutuc, E., Basu, D., Kim, S., Reddy, D. and MacDonald, A.H. (2010), "Graphene for CMOS and beyond CMOS applications", *Proc. IEEE.*, **98**(12), 2032-2046. https://doi.org/10.1109/JPROC.2010.2064151.

Bouadi, A., Bousahla, A.A., Houari, M.S.A., Heireche, H. and Tounsi, A. (2018), "A new nonlocal HSDT for analysis of

stability of single layer graphene sheet", *Adv. Nano Res., Int. J.*, **6**(2), 147. https://doi.org/10.12989/anr.2018.6.2.147.

Chhowalla, M., Jena, D. and Zhang, H. (2016), "Two-dimensional semiconductors for transistors", *Nature Rev. Mater.*, **1**(11), 16052. https://doi.org/10.1038/natrevmats.2016.52.

Chuan, M., Wong, K., Hamzah, A., Rusli, S., Alias, N., Lim, C. and Tan, M. (2020a), "Two-dimensional modelling of uniformly doped silicene with aluminium and its electronic properties", *Adv. Nano Res., Int. J.*, **9**(2), 105-112. http://doi.org/10.12989/anr.2020.9.2.105.

Chuan, M.W., Wong, K.L., Hamzah, A., Rusli, S., Alias, N.E., Lim, C.S. and Tan, M.L.P. (2020b), "2D honeycomb silicon: A review on theoretical advances for silicene field-effect transistors", *Curr. Nanosci.*, **16**(4), 595-607. https://doi.org/10.2174/1573413715666190709120019.

Chuan, M.W., Wong, K.L., Hamzah, A., Rusli, S., Alias, N.E., Lim, C.S. and Tan, M.L.P. (2020c), "Electronic properties and carrier transport properties of low-dimensional aluminium doped silicene nanostructure", *Physica E*, **116** 113731. https://doi.org/10.1016/j.physe.2019.113731.

Chuan, M.W., Wong, K.L., Hamzah, A., Rusli, S., Alias, N.E., Lim, C.S. and Tan, M.L.P. (2020d), "A review of the top of the barrier nanotransistor models for semiconductor nanomaterials", *Superlattice. Microst.*, **140** 106429. https://doi.org/10.1016/j.spmi.2020.106429.

Chuan, M., Wong, K., Hamzah, A., Rusli, S., Alias, N., Lim, C. and Tan, M. (2021), "Device modelling and performance analysis of two-dimensional AlSi3 ballistic nanotransistor", *Adv. Nano Res., Int. J.*, **10**(1), 91-99. http://doi.org/10.12989/anr.2021.10.1.091.

Datta, S. (1997), *Electronic Transport in Mesoscopic Systems*, Cambridge University Press, Cambridge, U.K. https://doi.org/10.1017/CBO9780511805776.

Datta, S. (2005), *Quantum transport: Atom to transistor*, Cambridge University Press, Cambridge, U.K. https://doi.org/10.1017/CBO9781139164313.

Ding, Y. and Ni, J. (2009), "Electronic structures of silicon nanoribbons", *Appl. Phys. Lett.*, **95**(8), 083115. https://doi.org/10.1063/1.3211968.

Ding, Y. and Wang, Y. (2013), "Density functional theory study of the silicene-like SiX and XSi3 (X = B, C, N, Al, P) honeycomb lattices: The various buckled structures and versatile electronic properties", *J. Phys. Chem. C.*, **117**(35), 18266-18278. https://doi.org/10.1021/jp407666m.

Gao, J., Zhang, J., Liu, H., Zhang, Q. and Zhao, J. (2013), "Structures, mobilities, electronic and magnetic properties of point defects in silicene", *Nanoscale*, **5**(20), 9785-9792. https://doi.org/10.1039/C3NR02826G.

Gert, A., Nestoklon, M. and Yassievich, I. (2015), "Band structure of silicene in the tight binding approximation", *J. Exp. Theo. Phys.*, **121**(1), 115-121. https://doi.org/10.1134/S1063776115060072.

Goossens, S., Navickaite, G., Monasterio, C., Gupta, S., Piqueras, J.J., Pérez, R., Burwell, G., Nikitskiy, I., Lasanta, T. and Galán, T. (2017), "Broadband image sensor array based on graphene–CMOS integration", *Nature Photonics*, **11**(6), 366-371. https://doi.org/10.1038/nphoton.2017.75.

Gupta, A., Sakthivel, T. and Seal, S. (2015), "Recent development in 2D materials beyond graphene", *Prog. Mater. Sci.*, **73,** 44-126. https://doi.org/10.1016/j.pmatsci.2015.02.002.

Guzmán-Verri, G.G. and Lew Yan Voon, L.C. (2007), "Electronic structure of silicon-based nanostructures", *Phys. Rev. B.*, **76**(7), 075131. https://doi.org/10.1103/PhysRevB.76.075131.

Harrison, W.A. (2004), *Elementary Electronic Structure: Revised*, World Scientific Publishing Company, Singapore. https://doi.org/10.1142/5432.

Huang, S., Kang, W. and Yang, L. (2013), "Electronic structure and quasiparticle bandgap of silicene structures", *Appl. Phys. Lett.*, **102**(13), 133106. https://doi.org/10.1063/1.4801309

IEEE (2018), International Roadmap for Devices and Systems (IRDS). https://irds.ieee.org/.

Ismail, R., Ahmadi, M.T. and Anwar, S. (2016), *Advanced Nanoelectronics*, CRC Press, Florida, U.S.A. https://doi.org/10.1201/9781315217185.

Johari, Z., Ahmadi, M.T., Chek, D.C.Y., Amin, N.A. and Ismail, R. (2010), "Modelling of graphene nanoribbon Fermi energy", *J. Nanomater.*, **2010** 14. https://doi.org/10.1155/2010/909347.

Jooq, M.K.Q., Mir, A., Mirzakuchaki, S. and Farmani, A. (2018), "Semi-analytical modeling of high performance nano-scale complementary logic gates utilizing ballistic carbon nanotube transistors", *Physica E*, **104** 286-296. https://doi.org/10.1016/j.physe.2018.08.008.

Kazmierski, T.J., Zhou, D. and Al-Hashimi, B.M. (2007). "A fast, numerical circuit-level model of carbon nanotube transistor", *2007 IEEE International Symposium on Nanoscale Architectures*. https://doi.org/10.1109/NANOARCH.2007.4400855.

Kim, R. and Lundstrom, M. (2008), *Notes on Fermi-Dirac Integrals, arXiv preprint arXiv:0811.0116*. http://nanohub.org/resources/5475.

Le Lay, G., Solonenko, D. and Vogt, P. (2018), *Synthesis of Silicene*, Springer. https://doi.org/10.1007/978-3-319-99964-7_5.

Lew Yan Voon, L., Zhu, J. and Schwingenschlögl, U. (2016), "Silicene: Recent theoretical advances", *Appl. Phys. Rev.*, **3**(4), 040802. https://doi.org/10.1063/1.4944631.

Lim, W.H., Hamzah, A., Ahmadi, M.T. and Ismail, R. (2017a), "Analytical study of the electronic properties of boron nitride nanosheet", *2017 IEEE Regional Symposium on Micro and Nanoelectronics (RSM)*. https://doi.org/10.1109/RSM.2017.8069115.

Lim, W.H., Hamzah, A., Ahmadi, M.T. and Ismail, R. (2017b), "Band gap engineering of BC2N for nanoelectronic applications", *Superlattice. Microst.*, **112**, 328-338. https://doi.org/10.1016/j.spmi.2017.09.040.

Lim, W.H., Hamzah, A., Ahmadi, M.T. and Ismail, R. (2018), "Performance analysis of one dimensional BC2N for nanoelectronics applications", *Physica E*, **102**, 33-38. https://doi.org/10.1016/j.physe.2018.04.005.

Lopez-Bezanilla, A. (2014), "Substitutional doping widens silicene gap", *J. Phys. Chem. C.*, **118**(32), 18788-18792. https://doi.org/10.1021/jp5060809.

Lundstrom, M.S. and Antoniadis, D.A. (2014), "Compact models and the physics of nanoscale FETs", *IEEE T. Electron Dev.*, **61**(2), 225-233. https://doi.org/10.1109/TED.2013.2283253.

Lundstrom, M. and Jeong, C. (2013), *Near-Equilibrium Transport: Fundamentals and Applications*, World Scientific Publishing Company, Singapore. https://doi.org/10.1142/7975.

Ma, L., Zhang, J.-M., Xu, K.-W. and Ji, V. (2014), "Nitrogen and Boron substitutional doped zigzag silicene nanoribbons: Ab initio investigation", *Physica E*, **60,** 112-117. https://doi.org/10.1016/j.physe.2014.02.013.

Mohan, B., Kumar, A. and Ahluwalia, P.K. (2014), "Electronic and optical properties of silicene under uni-axial and bi-axial mechanical strains: A first principle study", *Physica E*, **61,** 40-47. https://doi.org/10.1016/j.physe.2014.03.013.

Molle, A., Grazianetti, C., Tao, L., Taneja, D., Alam, M.H. and Akinwande, D. (2018), "Silicene, silicene derivatives, and their device applications", *Chem. Soc. Rev.*, **47**(16), 6370-6387. https://doi.org/10.1039/C8CS00338F.

Ni, Z., Zhong, H., Jiang, X., Quhe, R., Luo, G., Wang, Y., Ye, M., Yang, J., Shi, J. and Lu, J. (2014), "Tunable band gap and doping type in silicene by surface adsorption: towards tunneling transistors", *Nanoscale*, **6**(13), 7609-7618.

https://doi.org/10.1039/c4nr00028e.
Novoselov, K.S., Geim, A.K., Morozov, S.V., Jiang, D., Zhang, Y., Dubonos, S.V., Grigorieva, I.V. and Firsov, A.A. (2004), "Electric field effect in atomically thin carbon films", *Science*, **306**(5696), 666-669. https://doi.org/10.1126/science.1102896.
Rahman, A., Guo, J., Datta, S. and Lundstrom, M.S. (2003), "Theory of ballistic nanotransistors", *IEEE T. Electron Dev.*, **50**(9), 1853-1864. https://doi.org/10.1109/TED.2003.815366.
Schwierz, F., Pezoldt, J. and Granzner, R. (2015), "Two-dimensional materials and their prospects in transistor electronics", *Nanoscale*, **7**(18), 8261-8283. https://doi.org/10.1039/C5NR01052G.
Stpniak-Dybala, A., Dyniec, P., Kopciuszyski, M., Zdyb, R., Jałochowski, M. and Krawiec, M. (2019), "Planar silicene: a new silicon allotrope epitaxially grown by segregation", *Adv. Funct. Mater.*, **29**(50), 1906053. https://doi.org/10.1002/adfm.201906053.
Supriyo, D. (2017), *Lessons From Nanoelectronics: A New Perspective On Transport -Part A: Basic Concepts*, World Scientific Publishing Company, Singapore. https://doi.org/10.1142/10440-vol1.
Tang, Q. and Zhou, Z. (2013), "Graphene-analogous low-dimensional materials", *Prog. Mater. Sci.*, **58**(8), 1244-1315. https://doi.org/10.1016/j.pmatsci.2013.04.003.
Tao, L., Cinquanta, E., Chiappe, D., Grazianetti, C., Fanciulli, M., Dubey, M., Molle, A. and Akinwande, D. (2015), "Silicene field-effect transistors operating at room temperature", *Nature nanotechnol.*, **10**(3), 227. https://doi.org/10.1038/NNANO.2014.325.
Taur, Y., Mii, Y.-J., Frank, D.J., Wong, H.-S., Buchanan, D.A., Wind, S.J., Rishton, S.A., Sai-Halasz, G. and Nowak, E.J. (1995), "CMOS scaling into the 21st century: 0.1 μm and beyond", *IBM J. Res. Dev.*, **39**(1.2), 245-260. https://doi.org/10.1147/rd.391.0245.
Vogt, P., De Padova, P., Quaresima, C., Avila, J., Frantzeskakis, E., Asensio, M.C., Resta, A., Ealet, B. and Le Lay, G. (2012), "Silicene: compelling experimental evidence for graphenelike two-dimensional silicon", *Phys. Rev. Lett.*, **108**(15), 155501. https://doi.org/10.1103/PhysRevLett.108.155501.
Voon, L.L.Y., Lopez-Bezanilla, A., Wang, J., Zhang, Y. and Willatzen, M. (2015), "Effective Hamiltonians for phosphorene and silicene", *New J. Phys.*, **17**(2), 025004. https://doi.org/10.1088/1367-2630/17/2/025004.
Wang, Z., Feng, T. and Ruan, X. (2015), "Thermal conductivity and spectral phonon properties of freestanding and supported silicene", *J. Appl. Phys.*, **117**(8), 084317. https://doi.org/10.1063/1.4913600.
Wong, K.L., Chuan, M.W., Alias, N.E., Hamzah, A., Lim, C.S. and Tan, M.L.P. (2019), "Modeling of low-dimensional pristine and vacancy incorporated graphene nanoribbons using tight binding model and their electronic structures", *Adv. Nano Res., Int. J.*, **7**(3), 209-221. http://doi.org/10.12989/anr.2019.7.3.209.